

## Evaporation from a shallow water table: Diurnal dynamics of water and heat at the surface of drying sand

S. Assouline,<sup>1</sup> S. W. Tyler,<sup>2</sup> J. S. Selker,<sup>3</sup> I. Lunati,<sup>4</sup> C. W. Higgins,<sup>3</sup> and M. B. Parlange<sup>5</sup>

Received 2 December 2012; revised 30 April 2013; accepted 5 May 2013; published 8 July 2013.

[1] Accurate estimates of water losses by evaporation from shallow water tables are important for hydrological, agricultural, and climatic purposes. An experiment was conducted in a weighing lysimeter to characterize the diurnal dynamics of evaporation under natural conditions. Sampling revealed a completely dry surface sand layer after 5 days of evaporation. Its thickness was <1 cm early in the morning, increasing to reach 4–5 cm in the evening. This evidence points out fundamental limitations of the approaches that assume hydraulic connectivity from the water table up to the surface, as well as those that suppose monotonic drying when unsteady conditions prevail. The computed vapor phase diffusion rates from the apparent drying front based on Fick's law failed to reproduce the measured cumulative evaporation during the sampling day. We propose that two processes rule natural evaporation resulting from daily fluctuations of climatic variables: (i) evaporation of water, stored during nighttime due to redistribution and vapor condensation, directly into the atmosphere from the soil surface during the early morning hours, that could be simulated using a mass transfer approach and (ii) subsurface evaporation limited by Fickian diffusion, afterward. For the conditions prevailing during the sampling day, the amount of water stored at the vicinity of the soil surface was 0.3 mm and was depleted before 11:00. Combining evaporation from the surface before 11:00 and subsurface evaporation limited by Fickian diffusion after that time, the agreement between the estimated and measured cumulative evaporation was significantly improved.

**Citation:** Assouline, S., S. W. Tyler, J. S. Selker, I. Lunati, C. W. Higgins, and M. B. Parlange (2013), Evaporation from a shallow water table: Diurnal dynamics of water and heat at the surface of drying sand, *Water Resour. Res.*, 49, 4022–4034, doi:10.1002/wrcr.20293.

### 1. Introduction

[2] Evaporation from a shallow water table is a process important to water and salt budgets. The importance of the presence of a shallow water table on land-atmosphere fluxes was demonstrated theoretically [Gardner, 1958; Famiglietti and Wood, 1994; Salvucci and Entekhabi, 1995] and using numerical models [Rihani et al., 2010]. Further, the processes are very similar to those that describe evaporation from a drained profile where the groundwater level is far below the surface.

[3] Fundamentally, the process of evaporation involves the transport of liquid water, water vapor, and heat [de Vries, 1958; Whitaker, 1998; Milly, 1982; Parlange et al., 1998; Prat, 2002]. Two main stages characterize basically the process of evaporation from a bare soil, a liquid-flow controlled first stage where the soil flux is limited only by evaporative demand and hydraulic delivery of water to the surface, and a following stage controlled by vapor diffusion through the upper now dry medium, during which the evaporation rates decrease considerably and a receding vaporization plane can be identified [Van Brakel, 1980; Scherer, 1990; Lehmann et al., 2008].

[4] Insights into the complex process of evaporation from bare soil in the presence of a shallow water table have been gained largely from laboratory experiments [Rose et al., 2005; Gowing et al., 2006; Shokri and Salvucci, 2011]. Laboratory experiments that sought to simulate the diurnal fluctuations in temperature and humidity experienced by natural soils are scarce [Deol et al., 2012].

[5] Two mechanisms are relevant in the presence of shallow water table: evaporation at the land surface sustained by a continuous phase liquid flow from the water table; and subsurface evaporation maintained by diffusive vapor removal through the porous medium. In many simplified descriptions, based on the lack of a significant vapor pressure gradient when liquid phase water is present, these two processes are seen as mutually exclusive, which allows

<sup>1</sup>Institute of Soil, Water and Environmental Sciences, A.R.O., The Volcani Center, Bet-Dagan, Israel.

<sup>2</sup>Department of Geological Sciences and Engineering, University of Nevada, Reno, Reno, Nevada, USA.

<sup>3</sup>Department of Biological and Ecological Engineering, Oregon State University, Corvallis, Oregon, USA.

<sup>4</sup>Research Center for Terrestrial Environment, University of Lausanne, Lausanne, Switzerland.

<sup>5</sup>School of Architecture, Civil and Environmental Engineering, Ecole Polytechnique Federale de Lausanne (EPFL), Lausanne, Switzerland.

Corresponding author: S. Assouline, Institute of Soil, Water and Environmental Sciences, A.R.O., The Volcani Center, Bet-Dagan, Israel. (vwshmu@agri.gov.il)

for the derivation of simple analytical solutions to estimate evaporation. In the case where surface evaporation is predominant, for instance, one can use the simple solution for 1-D steady evaporation from a homogeneous soil profile with a shallow water table that can be derived from Darcy's law or Richards's equation [Gardner, 1958; Brutsaert, 2005]:

$$z = \int_0^{x=\psi} \frac{dx}{[1 + E/K(x)]}, \quad (1)$$

where  $z$  is the soil depth taken positive upward,  $z=0$  is the level of the water table, and  $z=L$  is the level of the soil surface;  $x$  is a dummy variable of integration representing the soil capillary head,  $\psi$ , which is here considered to be invariant in time and only dependent on position;  $K(\psi)$  is the hydraulic conductivity function (HCF); and  $E$  is the constant evaporation rate from the soil surface and also the flux throughout the profile due to the assumption that the system is at steady state.

[6] For certain expressions of  $K(\psi)$ , analytical solutions of equation (1) are available [see Gardner, 1958; Gardner and Fireman, 1958; Warrick, 1988; Brutsaert, 2005]. Perhaps, the most widely known solution is found taking  $K(\psi)$  to be represented by the exponential function [Gardner, 1958]:

$$K(\psi) = K_s e^{-\alpha_G \psi}, \quad (2)$$

where  $K_s$  is the saturated hydraulic conductivity and  $\alpha_G$  is a fitting parameter related to the pore size distribution of the medium [Ghezzehei et al., 2007]. The maximum steady-state rate of evaporation,  $E_{max}$ , can be expressed analytically as a function of the depth to the water table,  $L$ , given a specific air entry-value,  $\psi_a$ , and assuming an infinite value for  $\psi_{z=L}$  at the soil surface:

$$E_{max-G} = \frac{K_s}{\exp[\alpha_G(L - \psi_a)] - 1}. \quad (3)$$

[7] Exact solutions were also found for  $K(\psi)$  being represented by

$$K(\psi) = \frac{a}{b + |\psi|^c}, \quad (4)$$

where  $a$ ,  $b$ , and  $c$  are constants that can be considered as fitting parameters. Gardner [1958] presented solutions for  $c = 1, 1.5, 2, 3$ , and  $4$ . Warrick [1988] extended these solutions and proposed a general solution for  $c > 1$ . The resulting expression of  $E_{max}$  proposed by Warrick [1988] is

$$E_{max-W} = a \left[ \frac{(\pi/c)}{\sin(\pi/c)} \right]^c L^{-c}; \quad c > 1. \quad (5)$$

[8] The solutions presented in equations (3) and (5) assume the continuity of water films from the water table to the soil surface. This assumption stems from the definition of the HCF to be continuous in pressure head, with no representation of vapor flux (i.e., the only modeled pathway for soil to dry would be through removal of water through

films of flow). It is thus evident that the validity of such an assumption will depend on the specific combination between the depth of the water table and the hydraulic properties of the soil layer between that water table and the surface. When the hydraulic properties of the soils are known, balancing between, gravity, capillary, and viscous forces allows the evaluation of the characteristic length for which the assumption of water film continuity remains valid [Lehmann et al., 2008]. Based on that analysis, Shokri and Salvucci [2011] proposed the simplified definition of the maximum depth of the water table,  $L_{max}$ , that would remain hydraulically connected to the soil surface during a given evaporation event at rate  $E$ :

$$L_{max} = \frac{\psi_{max} - \psi_a}{1 + E/K} + \psi_a, \quad (6)$$

where  $\psi_{max}$  is the capillary head for which water films are disrupted. When the depth of the water table exceeds  $L_{max}$ , an evaporation front (or vaporization plane) will form below the soil surface, and the evaporation process will result from vapor diffusion from that vaporization plane through the dry layer up to the soil surface [Bristow and Horton, 1996; Saravanapavan and Salvucci, 2000; Shokri and Or, 2010]. The range of evaporation rates at the onset of this stage is relatively narrow, between 0.5 and 3.5 mm d<sup>-1</sup> [Shokri and Or, 2011]. The corresponding thickness of the dry layer above the vaporization plane also varies within a relatively narrow range, from 3 to 20 mm [Novak, 2010; Shokri and Or, 2011; Smits et al., 2012; Deol et al., 2012]. Applying Fick's law, the diffusive evaporation rate,  $E_{dif}$ , can be estimated following Moldrup et al. [2000] and Shokri et al. [2009]:

$$E_{dif} = \frac{\theta_a^{2.5}}{\varphi} D_o \frac{C_{sat} - C_{air}}{L_d}, \quad (7)$$

where  $\theta_a$  is the volumetric air content in the dry layer above the vaporization plane,  $\varphi$  is the soil porosity,  $D_o$  is the vapor diffusion coefficient in free air,  $C_{sat}$  is the saturated water vapor density at the vaporization plane,  $C_{air}$  is the water vapor density in the air above the soil surface, and  $L_d$  is the thickness of the dry soil layer (the distance from the vaporization plane to the soil surface). The power of 2.5 on air saturation is included to account for effects of tortuosity and cross-sectional area available for diffusion. A power of 2.33 could be applied instead if adopting the expression for tortuosity suggested by Millington and Quirk [1961], though given the uncertainties in many of the parameters and dimensions (e.g., where is the drying front); this adjustment would likely be below experimental detection in practice. An implicit assumption of equation (7) is that the system is at steady state so that the humidity profile is linear over  $L_d$ , as predicted by Fick's law. Departure from steady-state condition would affect the humidity profile and consequently the evaporation rate relative to the estimate from equation (7) [Rollins et al., 1954].

[9] Experimental evidence suggests that often, equation (7) tends to underestimate diffusive fluxes from drying porous media [Gurr et al., 1952; Taylor and Cavazza, 1954]. Cahill and Parlange [1998] reported that vapor fluxes

predicted by equation (7) were lower than the values derived from the field measurements by 1 order of magnitude. The discrepancy between data and predictions has led to the development of several models that could justify the introduction of a vapor-flux enhancement factor. A conceptual model involving small capillary-held pendular water bodies and local thermal gradient effects that could increase vapor flow velocity in the pores was already proposed by *Philip and de Vries* [1957]. *Philip and de Vries* [1957] limited the applicability of the suggested processes favoring vapor enhancement to a certain limiting water content that was not explicitly defined. *Gardner* [1958] estimated the potential increase of such processes to be 20% of the diffusive flux. *Ho and Webb* [1998] questioned the validity of these processes, and *Shokri et al.* [2009] provided a critical analysis of the enhancement concept during stage 2 evaporation. Their conclusion was that “with proper account of capillary flow, continuity and pathways, no enhancement factors are needed” [*Shokri et al.*, 2009; p. 8]. *Griffoll et al.* [2005] also found that soil-water and energy transport dynamics can be described without the use of empirical enhancing transport factors. Using a mechanistic pore-scale model of evaporation and condensation, *Shahraeeni and Or* [2012] showed that isolated liquid phase bridges reduce the gaseous diffusion path length, thus enhancing water vapor transport by approximately 10%.

[10] The possible influence of macroscopic temperature gradients within the drying profile was also raised. A thermal gradient can either assist or oppose diffusive flux, depending on its direction. Studying the influence of temperature gradients on the drying of pore networks, *Huinink et al.* [2002] have shown that the drying rate is enhanced significantly when the temperature of the evaporating surface is higher than the temperature at the bottom of the network. At the pore scale, *Shahraeeni and Or* [2012] showed that a mild local thermal gradient could affect the water vapor diffusion rate by only several percent when compared to isothermal diffusion. However, when upscaled to a sample scale, their results indicated that a mild assisting thermal gradient could double the water vapor diffusion rate compared to isothermal diffusion of an inert gas. Finally, thermally driven convective transport mechanisms could increase the vapor flux from the deeper layers to the soil surface [*Papendick et al.*, 1973; *Pikul and Allmaras*, 1984; *Whitaker*, 1998; *Bachmann et al.*, 2001].

[11] In most of the practical cases of evaporation from shallow water tables, the significant water losses due to evaporation will occur until the transition between the first and the second stages of the evaporation process. However, as the first stage of evaporation is likely to be short lived in natural conditions, an interesting additional phenomenon could be relevant: compensation effects due to the increase of the evaporation rate per unit of evaporating area when evaporation takes place from small pores filled of water that are surrounded by larger pores that are already dry [*Bange*, 1953; *Cooke*, 1967; *Shahraeeni et al.*, 2012]. This issue was investigated both experimentally and theoretically in the context of diffusion from perforated membranes but was shown to apply also in the case of evaporation from partially covered water surfaces [*Assouline et al.*, 2010a, 2011]. *Suzuki and Maeda* [1968] and *Schlünder* [1988] have proposed solutions showing how the evaporation rate from

drying porous media varied with the fraction of the wet area of the drying surface. Due to these compensation effects, the evaporation rate remains practically constant for a large range of relative wet surfaces and decreases only after a critical, limited, relative wet area is reached.

[12] All these processes might lead to the enhancement of the diffusive rate through the dry soil layer. They provided the framework for a series of studies suggesting different ways to evaluate empirically that “enhancement factor” needed to reconcile between estimates based on equation (7) and observations [*Cary*, 1964; *Jury and Letey*, 1979; *Cass et al.*, 1984]. In particular, we focus on the potential for impacts of cyclic thermal conditions typically found between day and night as a possible enhancement factor under natural conditions.

[13] The main objectives of this study are (i) to characterize the dynamics of the water and heat regimes at the vicinity of a naturally drying sand and to analyze its impact on the diffusion process through a dry layer; (ii) to compare detailed weighing lysimeter observations of the temporal distribution of evaporation with numerical model and analytical model predictions; and (iii) to analyze the process of drying during diurnal fluctuations in temperature and humidity experienced by natural soils.

## 2. Lysimeter Experiment

[14] A lysimeter experiment was carried out at the Ecole Polytechnique Federale de Lausanne using the Lysimeters Facility of the Laboratory of Environmental Fluid Mechanics and Hydrology, which is located in a 60 m × 60 m open-grass yard. Measurements were carried out in summer 2006 during two consecutive periods: from 29 June to 3 July (120 h) and from 10 to 19 July (240 h).

[15] The weighable lysimeter consisted of a polyester reinforced fiberglass tank of 2.50 m height and 1.20 m diameter, with a surface area of 1.13 m<sup>2</sup>. The lysimeter was placed on three high-accuracy loading cells (Hottinger and Baldwin Messtechnik GMBH, Germany), with a system resolution of 100 g, enabling measureable changes in lysimeter water content equivalent to 0.0885 mm. The lysimeter was installed below ground so that the rim corresponds to the ground level, and its surface is exposed to climatic forcing at the level of the surroundings. The bottom of the lysimeter was filled with a coarse drainage layer consisting of 25 cm of gravel topped with 25 cm of coarse sand. The remaining 200 cm were filled with local fine sand. Details on the sand mechanical composition and granulometry are provided in Appendix A and Figure A1. To achieve a homogenous packing, the lysimeter was filled through successive approximately 5 cm lifts each involving a gentle deposition of sand followed by a rise of the water table up to saturation.

[16] During the filling, the lysimeter was equipped with tensiometers and thermocouples providing information on capillary head and temperature. The capillary head was measured by means of fast response UMS mini tensiometers T5, with a cup diameter of 0.5 cm (UMS, Munich, Germany). These tensiometers were installed 10, 20, and 40 cm below the sand surface. The soil temperature was monitored based on copper-constantan thermocouples. The thermocouples were installed at 2, 10, 20, 40, and 60 cm below the sand surface. All the sensors were connected to data

loggers (Campbell CR5000) and data collected every 15 min to every 30 min.

[17] Tensiometers readings were corrected for temperature. The volumetric water content was estimated based on the tensiometer readings and the soil water retention curve (WRC; Appendix C).

### 2.1. Experimental Procedure

[18] The bottom part of the lysimeter allows addition or removal of water. During filling this was connected to domestic water supply. The water table level was monitored by means of a piezometer. Before each drying period, the lysimeter was completely saturated from the bottom and let drain to a zero-pressure water table set at  $z = -80$  cm. The lysimeter was covered by an air tight lid and let drain for several days (until no further drainage was seen which we refer to as quasi-steady-state conditions), allowing the formation of essentially hydrostatic initial conditions. At the beginning of each evaporation experiment, drainage was stopped and a no-flux condition imposed at the bottom of the lysimeter, and the lid that covered the lysimeter surface was removed to expose the sand surface to climatic forcing. The evaporation rates from the lysimeter were evaluated based on the hourly recorded changes in weight of the drying lysimeter.

### 2.2. Meteorological Data

[19] Climatic data from a micrometeorological station situated 10 m away from the lysimeter provided hourly data on global radiation, wind speed and direction, air temperature, and relative humidity at 2 m height. The climatic data corresponding to the first period are presented in Appendix B and Figure B1. They were used to estimate potential evaporation,  $E_p$ , at the site, following Allen *et al.* [1998]. This micrometeorological station failed to provide data for the second period. Therefore, corresponding  $E_p$  values for that period were estimated based on relative changes in daily  $E_p$  estimated by MeteoSwiss for the station at Pully, 7 km from the experimental site, that was found to be highly correlated with the micrometeorological station on-site ( $R^2 = 0.98$ ).

### 2.3. Hydraulic Properties

[20] The sand hydraulic properties were estimated in the laboratory using packed samples of the same media employed in the lysimeter. The drying WRC was measured using a sand table (Eijelkamp, Netherlands). The disturbed samples were packed at a bulk density of  $1.675 \text{ g cm}^{-3}$ , which corresponded approximately to the packing density of the lysimeter (porosity  $\varphi = 0.376$ ). The expression of van Genuchten [1980] for the WRC was fitted to the data. The saturated hydraulic conductivity,  $K_s$ , was measured using a constant head device. These samples were packed at a higher bulk density of  $1.83 \text{ g cm}^{-3}$ . The corrected values of  $K_s$  for the lower bulk density of the samples used for the measure of the WRC (and of the lysimeter) were computed following the model of Assouline [2006], resulting in an adjustment upward by a factor of 2.71. The HCF was estimated based on the model of Mualem [1976]. The hydraulic functions of the sand are presented in Appendix C and depicted in Figure C1.

### 2.4. Destructive Sample

[21] At the end of the first period, on 3 July, a destructive sampling of the upper layer of the dry sand surface of the

lysimeter was carried out. Syringe bodies of 2.5 cm diameter were gently pushed vertically into the sand surface at two different locations to a depth of just over 12 cm. As the samples were ejected from the syringes they were sectioned into segments of 2 cm length, and the gravimetric water content was estimated by weighing and oven-drying of the samples. The sampled midpoint depths were 1.1, 3.1, 4.9, 6.7, 8.5, 10.3, and 12.1 cm. The samples corresponding to the upper few centimeters were very dry, and their water content was estimated using a WP4 dew point potentiometer (Decagon Devices, Pullman, WA, USA). This destructive sampling was carried out at 2 to 3 h intervals, from 7:00 to 18:00, at 7:20, 10:00, 12:00, 14.45, and 18:00 h. A similar destructive sampling was carried out also at the end of the second period (19 July), but samples were taken only at 16:00 and at 6:00 the day after. The evolution of global radiation and air temperature and relative humidity during that day are shown in Figure B1 of Appendix B. Measurements were carried out in duplicates.

### 2.5. Numerical Simulations

[22] The ability of the standard approach to model coupled heat and moisture transfer to reproduce evaporation dynamics in the presence of a shallow water table was investigated by performing numerical simulations that mimic experimental conditions. Simulations were performed employing two widely used numerical codes: HYDRUS-1D [Simunek *et al.*, 2005] and its modified version that accounts for heat transport [Saito *et al.*, 2006]. The estimated hydraulic properties of the sand (Appendix C) were used. Estimated hourly  $E_p$  rates provided the upper boundary condition. A soil profile of 100 cm depth, with a space discretization of 1.0 cm, represented the flow domain. A no-flux condition at  $z = -100$  cm was used for the lower boundary. For the first period, initial condition corresponding to hydrostatic profile of  $\psi$  above the water table set at  $z = -80.0$  cm was implemented. For the second period, the initial condition corresponded to the profile developing after 6 days of draining with no evaporation from an initially saturated profile to a water table fixed at  $z = -80.0$  cm. For the simulations accounting for temperature effects, the default thermal properties for a loam soil were used as they better reproduced the measured temperature dynamics at the different depths. A uniform temperature profile was employed as the initial condition; measured soil surface temperatures were applied as upper boundary condition, and constant temperature of  $T = 23^\circ\text{C}$  at  $z = 0$  was assumed as a lower boundary condition. Time discretization was as follows: initial time step, 0.1 min; minimum time step, 0.01 min; and maximum time step, 1 min.

## 3. Results and Discussion

### 3.1. Evaporation Rates

[23] The cumulative measured evaporation during the two periods is depicted in Figure 1, along with the estimated cumulative potential evaporation,  $E_p$ . More water evaporated from the lysimeter during the first 5 days of the second period by comparison to the first period in spite of the lower cumulative  $E_p$ . This may have resulted from the fact that the atmospheric demand was weaker in the first days of the second period, allowing accommodation of the lower soil layers to changes at the surface, and leading to a

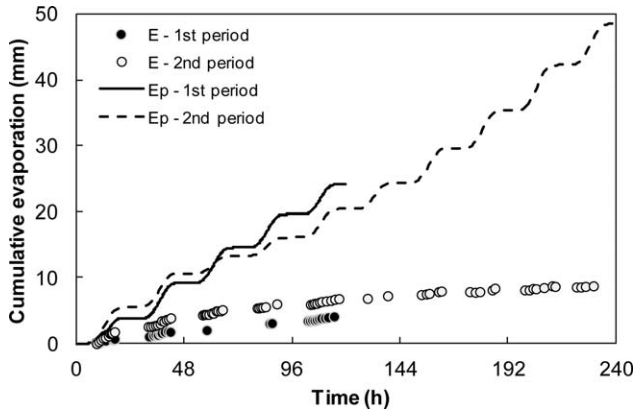


**Figure 1.** Measured cumulative evaporation during the two periods (symbols) and corresponding estimated cumulative potential evaporation (lines) estimated following *Allen et al.* [1998].

better and more efficient continuity of the liquid films from the wet deeper layers to the evaporating surface. A second reason is that the soil profile was wetter at the beginning of the second period, if 6 days of draining were not sufficient to generate essentially hydrostatic conditions.

[24] Simulated results for the two periods based on HYDRUS-1D neglecting temperature effects on soil-water relationships [*Gardner, 1955; Philip and de Vries, 1957; Nimmo and Miller, 1986; Hopmans and Dane, 1986; Grant and Bachman, 2002*] slightly overestimate cumulative evaporation over the whole period (Figure 2). *Saito et al.* [2006] developed a version of HYDRUS where temperature effects on soil-water surface tension and on the WRC were accounted for following *Nimmo and Miller* [1986]. Using that version improved the agreement between simulated and measured data, although a small discrepancy can still be observed at the end of the period.

[25] For the second period, the simulated results fail to reproduce the convex curvature of the measured cumula-

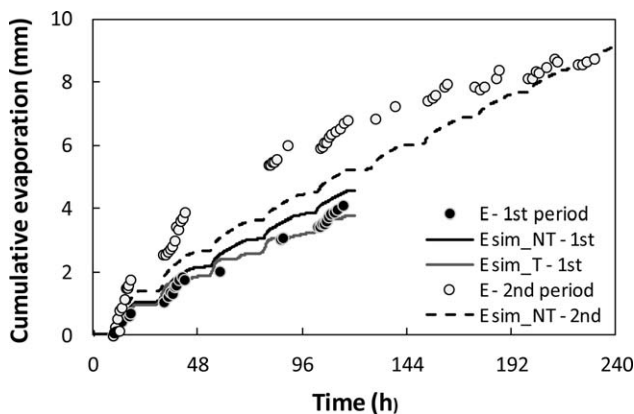


**Figure 2.** Measured cumulative evaporation during the two periods (symbols, E-1st and E-2nd periods) and corresponding simulated cumulative evaporation using HYDRUS-1D without accounting for temperature effect (black lines; *Esim\_NT*) and with accounting for temperature effects following *Saito et al.* [2006] (gray line; *Esim\_T-1st*).

tive evaporation and underestimated the water losses for practically the whole period and a more linear behavior is simulated, even though the predicted cumulative evaporation after 10 days concurred with the observed total. Notice that meteorological data for this period were less precise due to the lack of local measurements, replaced by data from the closest available (MeteoSwiss station of Pully, located about 7 km from the lysimeter site).

[26] To check the validity of the simulations, the dynamics of the measured temperature and water content at different depths within the soil profile are compared with the simulated ones (Figure 3). While the temperature values are measured directly, the water content values resulted from transforming tensiometer readings at the specific depths into volumetric water content,  $\theta$ , based on the soil WRC (Appendix C). The computed temperatures agree well in terms of both amplitude and phase with the measured values, indicating that heat is properly transported by the model, and that the initial and boundary thermal conditions and soil thermal properties applied are representative of the experimental setup. The overall agreement between simulated and measured water content values can be considered satisfactory, and this agreement improves as depth increases (Figure 3). When no effect of temperature is accounted for in the model, only slight daily variations are

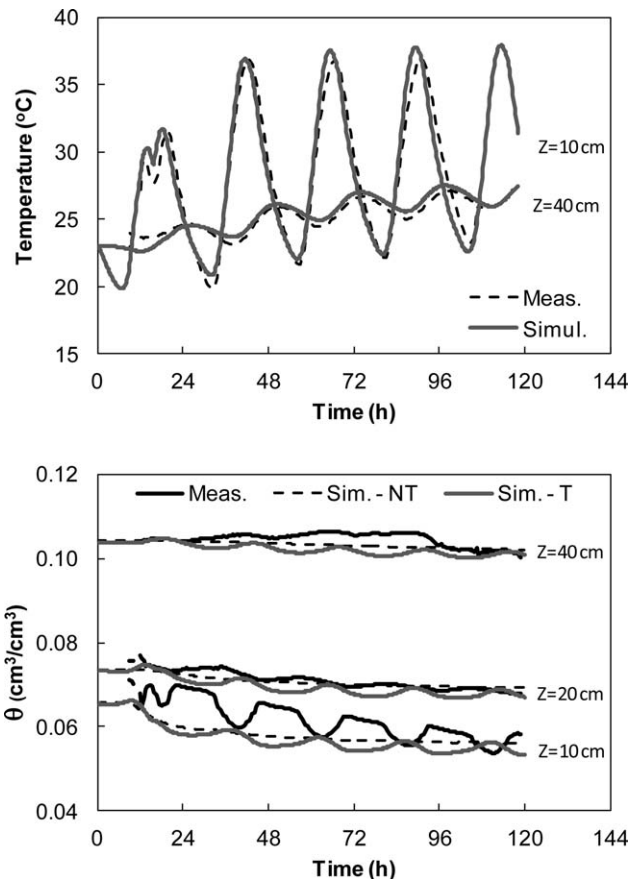


**Figure 3.** (upper) Measured and simulated soil temperature and (lower) volumetric water content at different depths within the lysimeter during the first period. Gray lines represent simulation results based on the HYDRUS-1D model of coupled water and heat transport.

simulated, and when this effect is considered, these variations increased in amplitude. However, scrutiny of the results reveals that the phase of the diurnal variations is opposite to those measured close to the soil surface. This is due to the fact that the simulated evaporative flux around noon was zero, when the simulated water content at the soil surface reached the model constraint of  $\theta_r$ . This illustrates the limit of the methods assuming water continuity in the solution domain under the conditions of the experiment.

[27] The numerical solution seems to indicate that hydraulic continuity in the lysimeter could be sustained from the water table at  $z = -80$  cm to the soil surface. According to equation (6), the maximum depth of a water table that could sustain hydraulic continuity to the soil surface is 31 cm, significantly shallower than the water table depth in the experiment. Assuming that equation (6) is accurate, hydraulic continuity is lost very near to the soil-atmosphere interface, and the water content there is lower than the residual value. Under such condition, the model solved numerically by HYDRUS is not applicable because it is unable to describe water fluxes once the simulated water content reaches the soil residual water content value.

[28] The steady-state solutions of *Gardner* [1958] (equation (3) above) and *Warrick* [1988] (equation (5) above) assume hydraulic connectivity between the water table and the evaporating surface to estimate the maximum evaporation rate. Figure 4 depicts the relationships between maximal daily evaporation rate and water table depth for these two solutions, along with the daily evaporation rates measured during both periods in this experiment (for water table depth of 80 cm). A striking difference, in terms of both trend and absolute values, can be observed between these two solutions, which agree for the single point corresponding to  $L = 72$  cm. The two relationships differ only in the expressions used to describe the HCF, namely, equation (2) versus equation (4), which were both fitted with a relatively similar agreement to the  $K(\psi)$  corresponding to the packed sand in the lysimeter (Appendix C). The large difference between the two solutions illustrates the importance of the hydraulic conductivity in quantitative estimates of evaporation rates. The measured values are below the curve

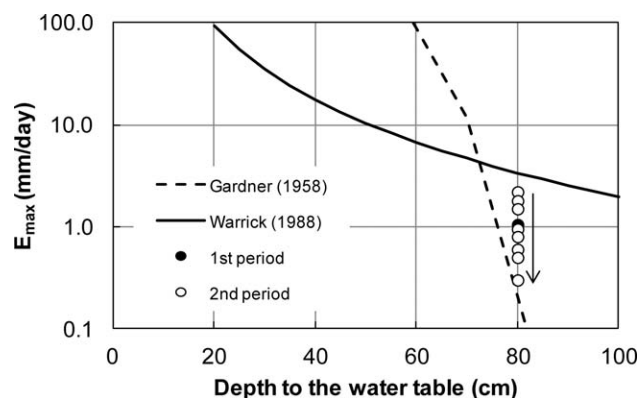


**Figure 4.** Relationships between maximal daily evaporation rate and water table depth based on steady-state solutions of *Gardner* [1958] (equation (3)) and *Warrick* [1988] (equation (5)) along with the daily evaporation rates measured during the two periods (symbols).

corresponding to equation (5) [*Warrick*, 1988] and above the curve corresponding to equation (3) [*Gardner*, 1958] during both experiment periods. This suggests that equation (3) is less realistic than equation (5) because measured evaporation rates are above the predicted maximum limit during the whole period.

[29] From the above, it is clear that there is an apparent contradiction between actual and expected behavior of the system under interest: on one hand, cumulative evaporation rates close to the measured ones could be simulated (Figure 2), indicating that the assumption of hydraulic continuity could still be valid; on the other hand, the depth of the water table is higher than the estimated maximal depth sustaining such a continuity, and the measured evaporation rates are below the maximal steady rate predicted by equation (5). We propose to analyze in the following the detailed information gathered during the destructive samplings to shed some light on this important issue.

### 3.2. Destructive Sampling Data

[30] The dynamics of the gravimetric water content with depth at the vicinity of the drying surface (upper 12 cm) measured during the destructive sampling carried out at the end of the first period (3 July) is depicted in Figure 5 (upper plot), which was produced using Kriging based on 35 data points (five discrete times and seven discrete depths). Two interesting features can be identified:

[31] (1) A completely dry sand layer exists at the surface after 5 days of evaporation. Its thickness was smaller early in the morning, but it gradually increased during the day up to 4–5 cm late in the evening. The location of a vaporization plane that has migrated into the soil profile during the day can be illustrated by the sharp yellow zone that represents approximately the residual water content value. This evidence points out fundamental limitations of the approaches that intrinsically assume hydraulic connectivity from the water table up to the surface. The analytical steady-state solutions of *Gardner* [1958] and *Warrick* [1988] (equations (3) and (5); Figure 4) as well as the numerical solution of the Richards equation via HYDRUS-1D (Figures 2 and 3) are not applicable to the near-surface conditions in the experiment. Since hydraulic continuity is inherently imposed on the system, simulated water contents are higher or equal to  $\theta_r$ , yielding a wetter soil profile with mild gradients (Figure 5, lower left plot). However, in the case where the dried layer is so thin that vapor diffusion across the dry soil depth is greater than potential film flow, the continuum approach may still be predictive.

[32] (2) A clear process of wetting of the soil profile abruptly halts at 9:00 in the morning at the 4 cm depth and deepens gradually to reach the 10 cm depth around noon (Figure 5; upper plot). This phenomenon was reported in several experimental studies [*Jackson*, 1973; *Cahill and Parlange*, 1998] and was related to the effect of temperature on the soil hydraulic properties and of temperature-gradient dynamics on liquid fluxes within the soil profile [*Assouline et al.*, 2010b].

[33] The simulated diurnal evolution of the temperature regime in the upper drying soil layer is presented in Figure 6. The heating of the soil surface and the heat propagation pattern with depth are clearly illustrated. The interesting feature is the inversion of temperature gradients with depth around

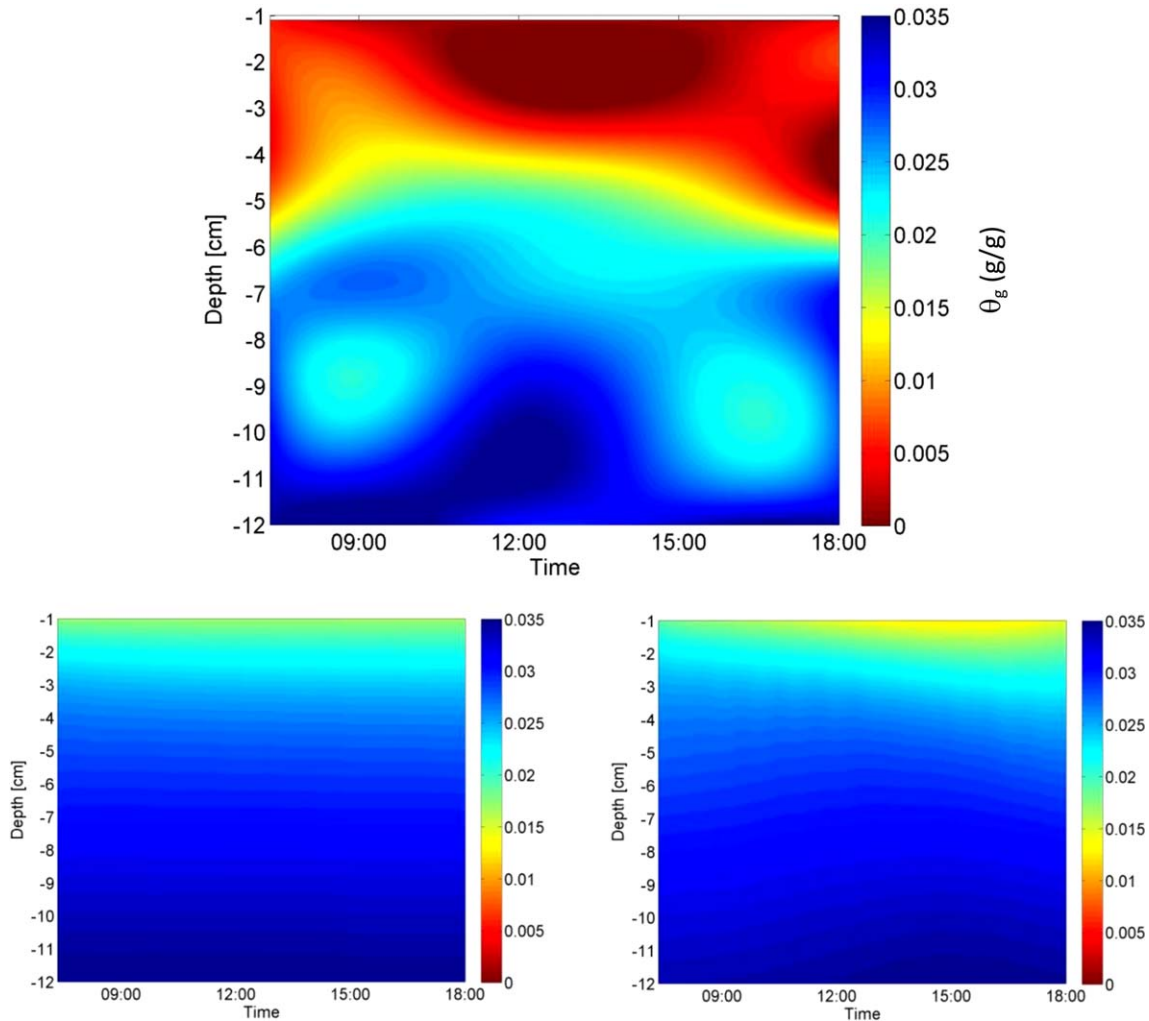


**Figure 5.** (upper) Dynamics of the distribution with depth of the gravimetric water content at the vicinity of the soil surface as measured during the destructive sampling at the end of the first period (3 July). The sampled midpoint depths were  $-1.1$ ,  $-3.1$ ,  $-4.9$ ,  $-6.7$ ,  $-8.5$ ,  $-10.3$ , and  $-12.1$  cm. The sampling times were at 7:20, 10:00, 12:00, 14.45, and 18:00 h. (lower left) Simulated dynamics of the distribution with depth of the gravimetric water content at the vicinity of the soil surface during the last day of the first period (3 July) using HYDRUS-1D without accounting for temperature effects. (lower right) Simulated dynamics of the distribution with depth of the gravimetric water content at the vicinity of the soil surface during the last day of the first period (3 July) using the HYDRUS-1D version that solve the coupled water and heat transport equations.

9:00: early in the morning, the soil surface is cooler than the deeper soil layer, and a temperature gradient opposing upward flux prevails. As the soil surface warms up, this trend is reversed and the soil surface became hotter than the deeper layers, inducing a temperature gradient that assists upward flux. Assouline *et al.* [2010b] suggested that this temperature gradient contributes to the wetting phenomenon depicted in Figure 5 (upper plot). A similar effect of temperature gradient on flow rates was demonstrated using simulation of drying at the pore scale [Shahraeeni and Or, 2012] and in pore network models [Huinink *et al.*, 2002]. Accounting for the dynamics of the temperature regime in the solution of the flow equations [Saito *et al.*, 2006] affects the water content regime only slightly (Figure 5; lower right plot), because liquid water is forced to remain hydraulically connected and may be also because of the nature of the temperature correc-

tions. A slightly dryer upper layer that deepens during the day is indeed simulated, and one could also recognize the wetting pattern that occurs at the 10 cm depth around noon. However, the predicted intensity of these processes is far from reproducing the data depicted in Figure 5 (upper plot).

[34] The gravimetric water content profiles measured during the two destructive samplings are shown in Figures 7a and 7b. In Figure 7a, the deepening of the dry layer during the day can be clearly seen. A similar trend was observed by Deol *et al.* [2012] and simulated by Novak [2010]. Also, the wetting phenomenon of the whole profile occurring during the night and early in the morning is well represented by the data. These profiles were used to estimate the thickness,  $L_{d_s}$ , of the dry layer, which is crucial in evaluating the diffusive rate of evaporation (equation (7)). It is evident that this could be a source of inaccuracy in

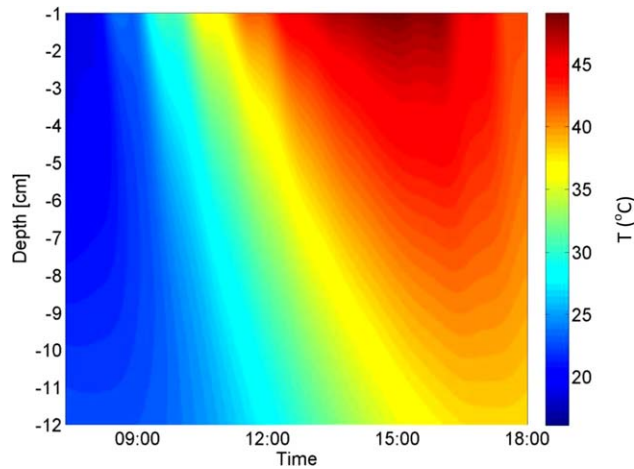


**Figure 6.** Simulated thermal regime with depth and time in the first 12 cm of soil during the last day of the first period (3 July) using the HYDRUS-1D representing coupled water and heat transport.

practical cases as it is difficult to determine  $L_d$  very accurately based on soil sampling and also because of its fractal nature [Shaw, 1987; Prat, 2002]. The destructive sampling at the end of the second period (Figure 7b) illustrates the further growth of the dry layer at the vicinity of the soil surface, and consequently, the increase in  $L_d$  which reduces the water vapor pressure gradient and, eventually, the diffusive evaporation rate.

[35] Continuous monitoring of lysimeter weight allows calculating the evaporation rates which corresponded to destructive sampling measurements. The destructive sampling data clearly indicate that the upper soil layer of the lysimeter was relatively humid (relative humidity of 100% at 1 cm depth) early in the morning (Figure 7a) and that it sig-

nificantly dried out during that day (Figure 5; upper plot). Consequently, the measured evaporation rates were at least in part constrained by the diffusion of water vapor through that dry layer, which could be estimated based on Fick's law (equation (7)). The climatic data of the micrometeorological station on-site provided the diurnal evolution of air temperature and relative humidity allowing the determination of the water vapor density above the soil surface,  $C_{air}$ . The data from the water vapor activity measurements using the WP4 allow determining the spatial and temporal distribution of relative humidity within the drying top soil. The simulations from the HYDRUS-1D version solving for water and heat movement enable the estimation of the spatial and temporal distribution of the soil temperature in the upper soil layer and allowed to account for soil temperature in the estimate of the diffusion coefficient. The diffusion coefficient,  $D_o$ , in equation (7) was corrected for temperature ( $D_o = 0.22(T/273)^{1.75}$  with  $T$  being the absolute mean temperature of the dry layer in kelvin during the day [Lide, 2006]). Based on information on soil relative humidity and temperature, the saturated water vapor density at the vaporization plane,  $C_{sat}$ , can be computed. Consequently, all the elements required to estimate diffusive rates based on Fick's law (equation (7)) are defined and evaluated, and the corresponding diffusive rates could be computed. The resulting estimated cumulative evaporation during the destructive sampling day is compared with the measured one using the lysimeter data in Figure 8a. The computed results underestimate the measured data approximately by a factor of three. In equation (7), the power of 2.5 on  $\theta_a$  accounts for the effect of tortuosity. Neglecting such effects, namely, assuming tortuosity  $\tau = 1$ , leads to a power of 2. The dotted curve depicts the cumulative evaporation computed following equation (7) with  $\theta_a^2$  replacing  $\theta_a^{2.5}$ . The resulting values are higher but still underestimate the measured data. The prescribed thickness of the dried layer,  $L_d$ , is uncertain

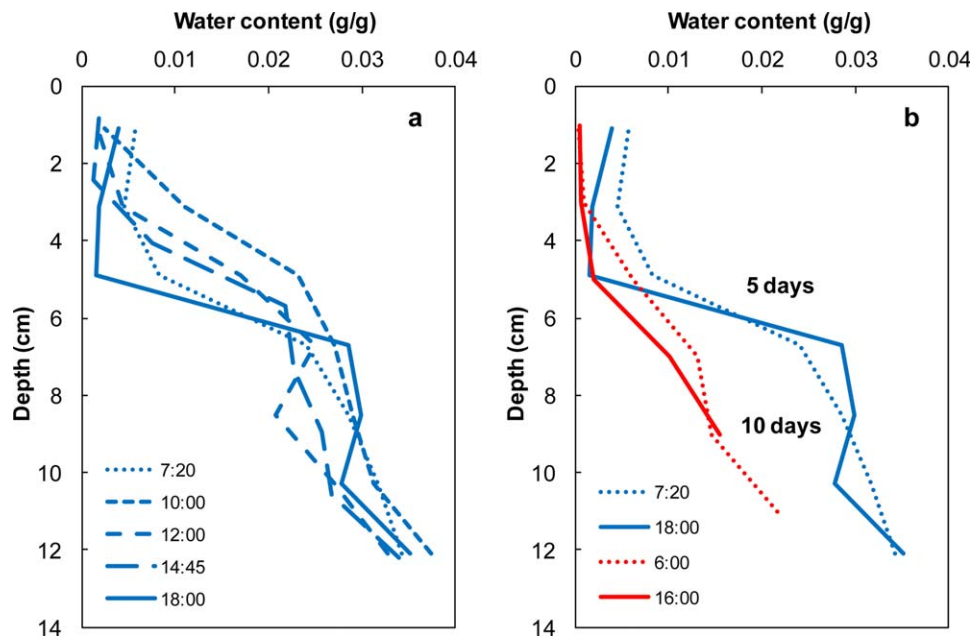


**Figure 7.** The gravimetric water content profiles measured during the (a) first and (b) second destructive samplings, at the end of the two drying periods.



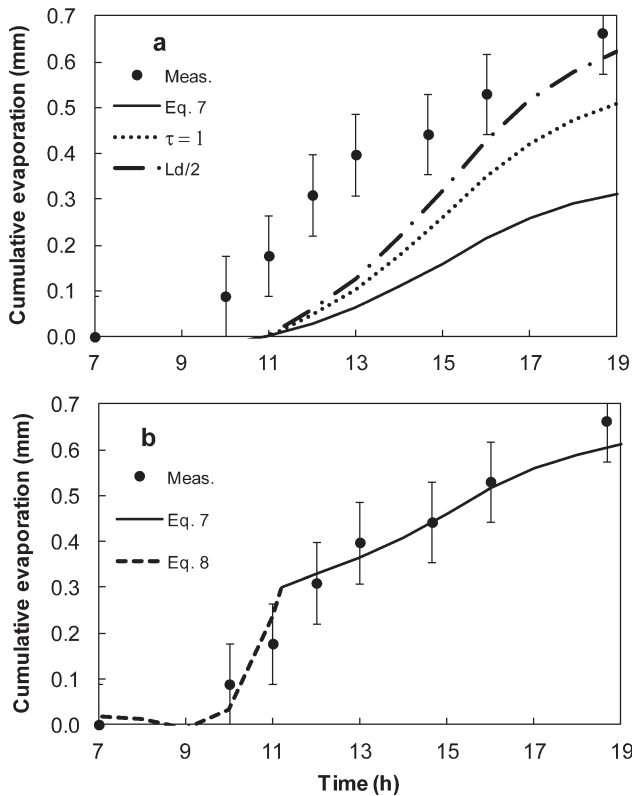


**Figure 8.** (a) Measured cumulative evaporation (symbols) during the last day of the first period (3 July), estimated cumulative evaporation based on equation (7) (solid line), assuming no tortuosity (dotted line), or accounting for half the thickness of the dry layer used in equation (7) (dashed line). (b) Measured cumulative evaporation (symbols) during the last day of the first period (3 July), estimated cumulative evaporation based on mass transfer (equation (8); dashed line), and estimated cumulative evaporation based on Fickian diffusion (equation (7); solid line).

and can also be a source of error. The sensitivity of equation (7) to  $L_d$  is illustrated by the dashed curve in Figure 8a that corresponds to equation (7) with  $(L_d/2)$ . Here also, the computed values underestimate the measured ones for most of the day. Based on the results in Figure 8a, one can conclude that the vapor diffusion from a subsurface vaporization plane alone cannot sustain the observed evaporation rate, unlike that reported by *Shokri et al.* [2009]. Unlike the present study, where large diurnal variations in both temperature and temperature gradient occurred, *Shokri et al.* [2009] considered evaporation under constant temperature and constant gradients, and the vaporization plane has a dominant control on the process in that case.

[36] These results also illustrate why additional processes that could enhance the diffusion intensity were suggested in the past [*Philip and de Vries*, 1957; *Cary*, 1964; *Jury and Letey*, 1979; *Cass et al.*, 1984] and are still investigated [*Lu et al.*, 2011; *Shahraeeni and Or*, 2012]. In our case, and during most of the day, a very dry layer was observed at the vicinity of the soil surface (Figures 5 and 7a). Therefore, pendular water bodies suggested by *Philip and de Vries* [1957] could not be present and play any role.

Similarly, the compensation effect suggested by *Suzuki and Maeda* [1968] and by *Schlünder* [1988] was not applicable in this case. Consequently, based on the destructive sampling data, none of the suggested processes capable of enhancing diffusion could be appropriately applied. Most importantly, the diffusion equation (with or without tortuosity), with its inherent assumption of a linear profile in relative humidity (equation (7)), cannot accurately represent the unsteady conditions resulting from the diurnal fluctuations in temperature and humidity experienced by natural soils during drying, particularly at the transition between day and night.

[37] We suggest here that the observed drying process can be explained by three distinct phases that cycle daily. For the purposes of explanation, we start in late afternoon, when the atmospheric evaporative demand decreases drastically and redistribution of the water content within the upper soil layer takes place, humidifying the very dry soil layer at the soil surface at the end of the day. In addition, at nighttime, the upper soil is cooled by upward long-wave radiation, and convective exchange with the relatively cool air. Through the course of the night, the air temperature drops, increasing relative humidity significantly, while the soil continues to be cooled to temperatures well below that of the air due to loss of long-wave radiation. This provides conditions for condensation of the water vapor saturated pores of the upper layer, and under certain climatic conditions, condensation at the surface as well.

[38] The second phase of the process is dominated by the evaporation of the water accumulated over nighttime. This water, being close to the surface, is readily available to satisfy the atmospheric evaporative demand. Based on the data from the destructive samplings, we can see that at sunrise, the upper soil layer is saturated with water vapor, and the upper 2 cm of the soil profile are at their wettest condition (Figure 7a). We postulate that this water accumulated during the night evaporates directly into the atmosphere during the morning hours, when the soil surface is heated, the air gets warmer and drier, and windier conditions develop (Figure C1). Even if this process is dominated by diffusion, it can sustain relatively high rates since the length of the diffusive path is still quite small.

[39] The third phase of the soil-water cycle starts when the water stored during the night is completely depleted and water for evaporation is provided by the vaporization plane below the subsurface. This water must be removed from the long-term drying front by diffusion through the now dry upper soil layer. Here the water loss is largely limited by liquid water supply to the vaporization plane by upward flow and by the vapor flux that can be generated due to Fickian gas diffusion through the dry layer. The beginning of the new cycle can be seen in the data corresponding to time 18:00 in Figure 7a, which reveal the beginning of a new rewetting process.

[40] Following *Brutsaert* [2005], we express the mass transfer process depleting the stored water during nighttime early in the morning by the equation:

$$E_{mt} = Ce \rho u (C_{sat} - C_{air}), \quad (8)$$

where  $E_{mt}$  is the mass transfer evaporation rate,  $\rho$  is the density of air;  $u$  is the mean wind velocity at a reference

height,  $C_{sat}$  is the saturated water vapor density at the soil surface,  $C_{air}$  is the water vapor density in the air above the soil surface, and  $C_e$  is the water vapor transfer coefficient that can be determined theoretically or empirically [Brutsaert, 2005]. Based on the available data from the destructive samplings, the empirical value of  $C_e = 4.75 \times 10^{-3}$  (corresponding to cumulative  $E_{mt}$  expressed in mm) led to a good agreement between the estimated values resulting from equation (8) and measured data corresponding to the morning hours (Figure 8b). The convex trend reflects the increase in wind speed that characterized that morning (last day shown in Figure C1), which affects  $E_{mt}$  (equation (8)).

[41] Once the stored water originating from nighttime redistribution and condensation is depleted, evaporation becomes a diffusion process that can be described by equation (7). The cumulative  $E_{dif}$  values resulting from equation (7), translated vertically by a total amount of nighttime water equal to 0.3 mm, are depicted in Figure 8b. The agreement with the measured data is quite good. Graphically, from the intersection between the curves representing the two processes, we can estimate a total amount of nighttime-accumulated water of approximately 0.25–0.3 mm, which was depleted around 11:00.

[42] Further investigation is needed to establish in a more rigorous way the proposed solution and to derive theoretical expressions for estimating  $C_e$  under daily cycles of drying.

#### 4. Summary and Conclusion

[43] Evaporation from a shallow water table under natural conditions was studied by means of a lysimeter experiment where the water table was set 80 cm below the soil surface. The well-established methods applied to describe the process and to quantify water losses via evaporation, namely, the analytical steady-state solutions of Gardner [1958] and Warrick [1988] or the standard numerical solution assume hydraulic continuity between the water table and the soil surface. A series of destructive sampling carried out 5 days after the onset of evaporation revealed the presence of a dry layer at the vicinity of the soil surface during most of the day, thus questioning the validity of these methods relatively early in the drying process.

[44] The thickness of the dry layer presented a significant variation during the day, being less than 1 cm thick early in the morning and increasing up to a 5 cm thickness late in the evening. This diurnal variation was related to the spatial and temporal distribution of the temperature gradient within the dry layer which presented a transition from positive and opposing temperature gradient at night to negative and assisting temperature gradient in the morning when the soil surface warmed up quicker than deeper soil layers.

[45] Because of the presence of that dry soil layer at the surface, the main physical process that could contribute to water losses from the lysimeter is diffusion of water vapor through the dry layer. Diffusion rates estimated based on Fick's law tend to underestimate the measured rates by a factor of three. Inherent to Fick's law is the assumption that the system is at steady state so that the humidity profile is linear over the dry layer.

[46] We have proposed, instead, that two rather than one single process rule natural evaporation resulting from daily

fluctuations of climatic variables: evaporation from the soil surface directly into the atmosphere during the early morning hours that could be simulated using a mass transfer approach, and subsurface evaporation limited by Fickian diffusion afterward, until the late afternoon. The first process depletes the water accumulated at the vicinity of the soil surface during nighttime redistribution and condensation. Once this amount of water, which will depend on the prevailing conditions in the soil-atmosphere system, is depleted, Fickian diffusion becomes the main process and the daily buildup of the dry layer takes place until late afternoon. Such an approach was successfully applied for the lysimeter experiment data. Invoking these two observed mechanisms of evaporation eliminates the need for artificial enhancement factors to achieve a good agreement between estimates and measured data. Our measurements suggest that traditional soil physics processes are able to explain the observed dynamics. However, widely employed models lack a sufficiently accurate description of vapor dynamics that would allow for night condensation and early morning evaporation near the surface, which have been conjectured in this paper.

#### Appendix A: Mechanical Analysis of Sand

[47] The sand used in the lysimeter contained 98% sand, 1% silt, and 1% clay. The grain size distribution was determined using a series of sieves. The distribution corresponding to grain size  $<2$  mm is depicted in Figure A1. The remaining fraction completing the distribution to 100% was characterized by a maximal grain size  $<10$  mm.

#### Appendix B: Climatic Data at the Experimental Site During the First Period

[48] A micrometeorological station on-site provided standard climatic data for the first period of the experiment. These data are depicted in Figure B1.

#### Appendix C: Hydraulic Properties of Sand

[49] The WRC of the sand was measured under laboratory conditions using a sand table (Eijelkamp, Netherlands).

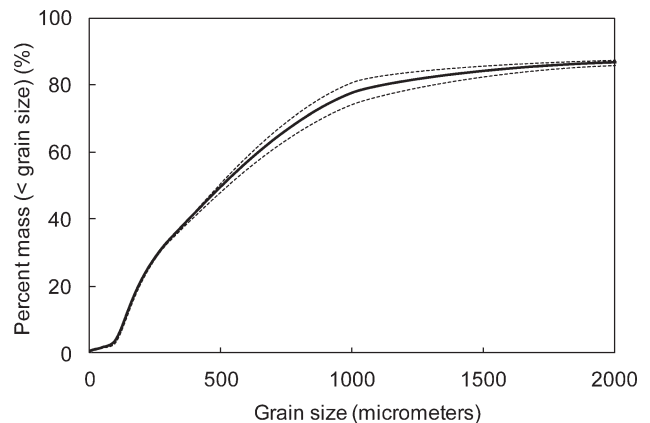


**Figure A1.** Cumulative grain size distribution of the sand used in the lysimeter.

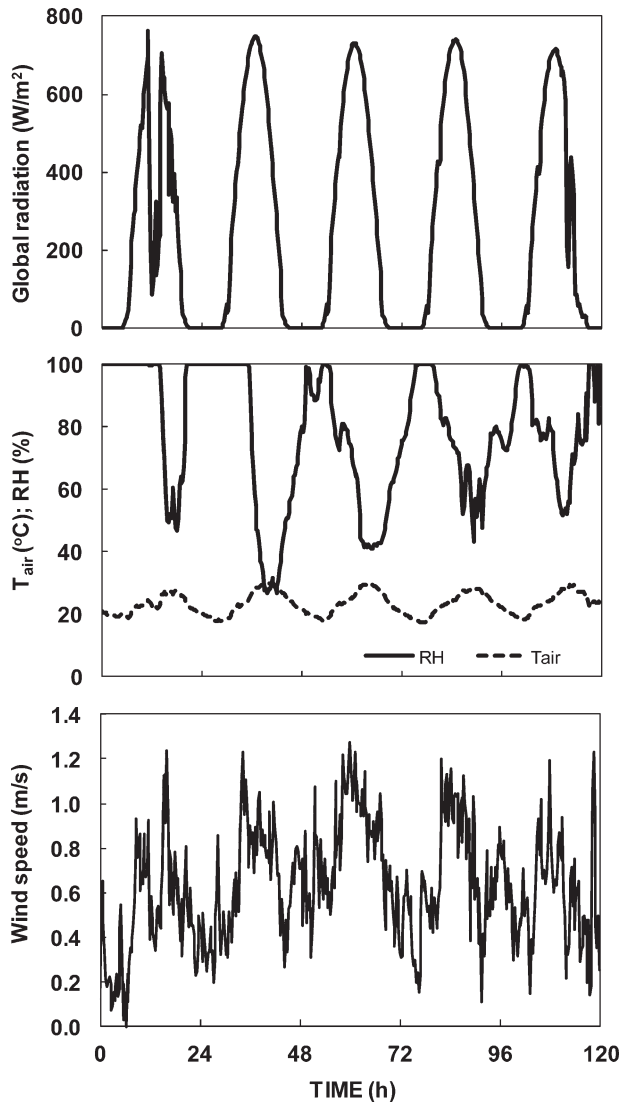


**Figure B1.** Climatic data characterizing the first period.

Disturbed soil samples were prepared at a bulk density of  $1.675 \pm 0.05 \text{ g cm}^{-3}$  and installed on the clothing of the sand table. Thirty-two samples were prepared and two samples were taken and weighted at each suction step to avoid replacing the samples after weighing, which could alter the good connectivity between the sample and the clothing. The samples were saturated, and the drying curve was measured by weighing the samples and estimating the water content after steady-state conditions were reached at different suctions achieved by successive lowering of the height of the free water level connected to the sand table. The expression of *van Genuchten* [1980] for the WRC was fitted to the measured data:

$$\theta(\psi) = (\theta_s - \theta_r) \left( \frac{1}{[1 + (\alpha|\psi|^n)^{1-1/n}]^n} \right) + \theta_r, \quad (\text{C1})$$

where  $\theta$  is the water content,  $\psi$  is the corresponding capillary head,  $\theta_s$  and  $\theta_r$  are the saturated and residual water contents, respectively, and  $\alpha$  and  $n$  are fitting parameters.

**Table C1.** Parameters Corresponding to the Estimated Hydraulic Functions of the Sand in the Lysimeter According to Equations (C1)–(C3)

	$\theta_s$ ( $\text{cm}^{-3} \text{ cm}^{-3}$ )	$\theta_r$ ( $\text{cm}^{-3} \text{ cm}^{-3}$ )	$\alpha$ ( $\text{cm}^{-1}$ )	$n$	$K_{s,WRC}$ ( $\text{cm h}^{-1}$ )
Sand	0.376	0.02	0.086	2.14	79.1

The corresponding values are presented in Table C1.

[50] The WRC of the sand packed in the lysimeter was estimated to be represented by equation (C1) as its packing bulk density after consolidation resulting from several saturation and drainage cycles was approximately equal to that of the disturbed samples used in the laboratory.

[51] The saturated hydraulic conductivity,  $K_s$ , of disturbed samples at a bulk density of  $1.83 \pm 0.04 \text{ g cm}^{-3}$  was measured in the laboratory in four replicates using a constant head device. The result was  $K_s = 29.2 \pm 3.0 \text{ cm h}^{-1}$ . To account for the effect of differences in packing soil bulk density, the measured values of  $K_s$  were corrected relatively to the bulk density of WRC measurement according to the model proposed by *Assouline* [2006]:

$$K_{s,WRC} = K_s \left( \frac{\varphi_{WRC}}{\varphi} \right)^3 \left( \frac{\rho_{WRC}}{\rho} \right)^{-3}, \quad (\text{C2})$$

where  $\varphi$  is the porosity taken equal to  $\theta_s$ ,  $\rho$  is the soil bulk density, and the index WRC correspond to the experimental conditions when the WRC was measured. The resulting corrected value is thus  $K_{s,WRC} = 79.1 \pm 8.1 \text{ cm h}^{-1}$ .

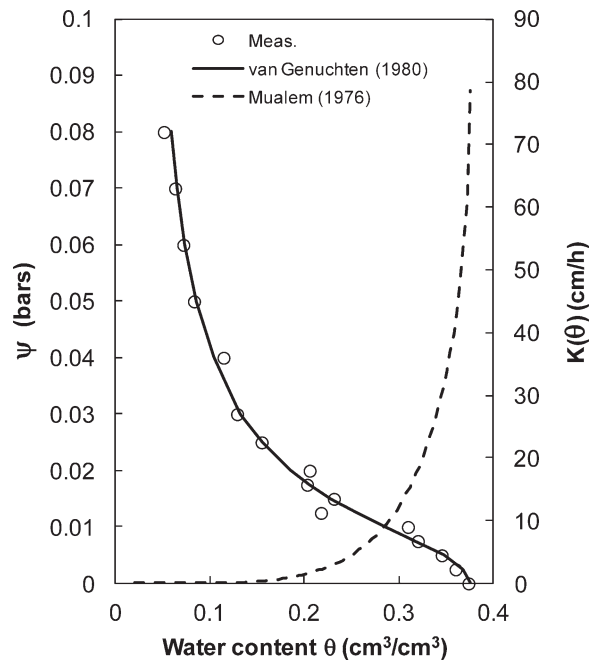


**Figure C1.** Measured WRC of the sand (symbols) and the fitted curve based on *van Genuchten* [1980] expression, and the corresponding HCF based on *Mualem* [1976] model.

[52] The HCF of the sand in the lysimeter was estimated based on the application of the model of *Mualem* [1976] to the *van Genuchten* [1980] expression of the WRC:

$$K(S_e) = K_{sWRC} S_e^{0.5} \left[ 1 - \left( 1 - S_e^{(1/m)} \right)^m \right]^2, \quad (C3)$$

where  $S_e = (\theta - \theta_r) / (\theta_s - \theta_r)$  is the effective saturation degree and  $m = 1 - 1/n$ .

[53] The resulting hydraulic functions of the sand are depicted in Figure C1.

[54] **Acknowledgments.** The authors wish to acknowledge Shmulik Friedman and Marc Prat for their insightful comments. The authors also thank Martin Tromp, Elisabeth Kiener, and Hendrik Huwald for their technical assistance. The constructive comments of Graham Sander (Editor) and anonymous AE and reviewers are also gratefully acknowledged.

## References

- Allen, R. G., L. S. Pereira, D. Raes, and M. Smith (1998), Crop evapotranspiration—Guidelines for computing crop water requirements, *FAO Irrig. Drain. Pap.* 56, FAO—Food and Agric. Organ. of the U. N., Rome.
- Assouline, S. (2006), Modeling the relationship between soil bulk density and the hydraulic conductivity function, *Vadose Zone J.*, 5, 697–705, doi:10.2136/vzj2005.0084.
- Assouline S., K. Narkis, and D. Or (2010a), Evaporation from partially covered water surfaces, *Water Resour. Res.*, 46, W10539, doi:10.1029/2010WR009121.
- Assouline, S., K. Narkis, S. W. Tyler, I. Lunati, M. B. Parlange, and J. S. Selker (2010b), On the diurnal soil water content dynamics during evaporation using dielectric methods, *Vadose Zone J.*, 9, 709–718, doi:10.2136/vzj2009.0109.
- Assouline, S., K. Narkis, and D. Or (2011), Evaporation suppression from water reservoirs—Efficiency considerations of partial covers, *Water Resour. Res.*, 47, W07506, doi:10.1029/2010WR009889.
- Bachmann, J., R. Horton, and R. R. van der Ploeg (2001), Isothermal and nonisothermal evaporation from four sandy soils of different water repellency, *Soil Sci. Soc. Am. J.*, 65, 1599–1607.
- Bange, G. G. J. (1953), On the quantitative explanation of stomatal transpiration, *Acta Bot. Neer.*, 2, 255–296.
- Bristow, K. L., and R. Horton (1996), Modeling the impact of partial surface mulch on soil heat and water flow, *Theor. Appl. Climatol.*, 54, 85–98.
- Brutsaert, W. (2005), *Hydrology—An Introduction*, Cambridge Univ. Press, Cambridge, U. K.
- Cahill, A. T., and M. B. Parlange (1998), On water vapor transport in field soils, *Water Resour. Res.*, 34, 731–739.
- Cary, J. W. (1964), An evaporation experiment and its irreversible thermodynamics, *Int. J. Heat Mass Transfer*, 7, 531–538, doi:10.1016/0017-9310(64)90050-X.
- Cass, A., G. S. Campbell, and T. L. Jones (1984), Enhancement of thermal water vapor diffusion in soil, *Soil Sci. Soc. Am. J.*, 48, 25–32.
- Cooke, J. R. (1967), Some theoretical considerations in stomatal diffusion: A field-theory approach, *Acta Biotheor.*, XVII, 95–124.
- de Vries, D. A. (1958), Simultaneous transfer of heat and moisture in porous media, *Eos Trans. AGU*, 39, 909–916.
- Deol, P., J. Heitman, A. Amoozegar, T. Ren, and R. Horton (2012), Quantifying non-isothermal sub-surface soil water evaporation, *Water Resour. Res.*, 48, W11503, doi:10.1029/2012WR012516.
- Famiglietti, J., and E. Wood (1994), Application of multiscale water and energy balance models on a tallgrass prairie, *Water Resour. Res.*, 30, 3079–3093, doi:10.1029/94WR01499.
- Gardner, R. (1955), Relations of temperature to moisture tension of soils, *Soil Sci.*, 79, 257–265.
- Gardner, W. R. (1958), Some steady-state solutions of the unsaturated moisture flow with applications to evaporation from a water table, *Soil Sci.*, 85, 228–232, doi:10.1097/00010694-195804000-00006.
- Gardner, W. R., and M. Fireman (1958), Laboratory studies of evaporation from soil columns in the presence of a water table, *Soil Sci.*, 85, 244–249, doi:10.1097/00010694-195805000-00002.
- Ghezzehei, T. A., T. J. Kneafsey, and G. W. Su (2007), Correspondence of the Gardner and van Genuchten–Mualem relative permeability function parameters, *Water Resour. Res.*, 43, W10417, doi:10.1029/2006WR005339.
- Gowing, J. W., F. Konukcu, and D. A. Rose (2006), Evaporative flux from a shallow watertable: The influence of a vapour–liquid phase transition, *J. Hydrol.*, 321, 77–89, doi:10.1016/j.jhydrol.2005.07.035.
- Grant, S. A., and J. Bachmann (2002), Effect of temperature on capillary pressure, in *Environmental Mechanics, Water, Mass and Energy Transfer in the Biosphere, Geophys. Monogr. Ser.*, vol. 129, edited by P. A. C. Raats, D. E. Smiles, and A. W. Warrick, pp. 199–212, AGU, Washington, D. C.
- Griffoll, J., J. M. Gastó, and Y. Cohen (2005), Non-isothermal soil water transport and evaporation, *Adv. Water Resour.*, 28, 1254–1266.
- Gurr, C. G., T. J. Marshall, and J. T. Hutton (1952), Movement of water in soil due to a temperature gradient, *Soil Sci.*, 74, 335–345, doi:10.1097/00010694-195211000-00001.
- Ho, C. K., and S. W. Webb (1998), Review of porous media enhanced vapor-phase diffusion mechanisms, models, and data—Does enhanced vapor-phase diffusion exist?, *J. Porous Media*, 1(1), 71–92.
- Hopmans, J. W., and J. H. Dane (1986), Temperature dependence of soil hydraulic properties, *Soil Sci. Soc. Am. J.*, 50, 4–9.
- Huinink, H. P., L. Pel, M. A. J. Michels, and M. Prat (2002), Drying processes in the presence of temperature gradients. Pore-scale modeling, *Eur. Phys. J. E*, 9, 487–498, doi:10.1140/epje/i2002-10106-1.
- Jackson, R. D. (1973), *Diurnal changes in soil water content during drying, in Field Soil Water Regime*, edited by R. R. Bruce et al., pp. 37–55, Soil Science Society of America, Madison, Wis.
- Jury, W. A., and J. Letey Jr. (1979), Water vapor movement in soil: Reconciliation of theory and experiment, *Soil Sci. Soc. Am. J.*, 43, 823–827.
- Lehmann, P., S. Assouline, and D. Or (2008), Characteristic lengths affecting evaporative drying of porous media, *Phys. Rev. E*, 77, 056309, doi:10.1103/PhysRevE.77.056309.
- Lide, D. R. (Ed.) (2006), *Handbook of Chemistry and Physics*, 87th ed., CRC Press, New York.
- Lu, S., T. Ren, Z. Yu, and R. Horton (2011), A method to estimate the water vapor enhancement factor in soil, *Eur. J. Soil Sci.*, 62(4), 498–504.
- Millington, R. J., and J. P. Quirk (1961), Permeability of porous media, *Trans. Faraday Soc.*, 57, 1200–1207.
- Milly, P. C. D. (1982), Moisture and heat transport in hysteretic, inhomogeneous porous media: A matrix head-based formulation and a numerical-model, *Water Resour. Res.*, 18, 489–498.
- Moldrup, P., T. Olesen, J. Gamst, P. Schjønning, T. Yamaguchi, and D. E. Rolston (2000), Predicting the gas diffusion coefficient in repacked soil: Water-induced linear reduction model, *Soil Sci. Soc. Am. J.*, 64, 1588–1594.
- Mualem, Y. (1976), A new model for predicting the hydraulic conductivity of unsaturated porous media, *Water Resour. Res.*, 12(3), 513–522, doi:10.1029/WR012i003p00513.
- Nimmo, J. R., and E. E. Miller (1986), The temperature dependence of isothermal moisture vs. potential characteristics of soils, *Soil Sci. Soc. Am. J.*, 50, 1105–1113.
- Novak, M. D. (2010), Dynamics of the near-surface evaporation zone and corresponding effects on the surface energy balance of a drying bare soil, *Agric. For. Meteorol.*, 150, 1358–1365.
- Papendick, R. I., M. J. Lindstrom, and V. L. Cochran (1973), Soil mulch effects on seedbed temperature and water during fallow in eastern Washington, *Soil Sci. Soc. Am. J.*, 37, 307–314.
- Parlange, M. B., A. T. Cahill, D. R. Nielsen, J. W. Hopmans, and O. Wendroth (1998), Review of heat and water movement in field soils, *Soil Tillage Res.*, 47, 5–10.
- Philip, J. R., and D. A. de Vries (1957), Moisture movement in porous materials under temperature gradients, *Eos Trans. AGU*, 38, 222–232.
- Pikul, J. L., Jr., and R. R. Allmaras (1984), A field comparison of null-aligned and mechanistic soil heat flux, *Soil Sci. Soc. Am. J.*, 48, 1207–1214.
- Prat, M. (2002), Recent advances in pore-scale models for drying of porous media, *Chem. Eng. J.*, 86, 153–164.
- Rihani, J. F., R. M. Maxwell, and F. K. Chow (2010), Coupling ground-water and land surface processes: Idealized simulations to identify effects of terrain and subsurface heterogeneity on land surface energy fluxes, *Water Resour. Res.*, 46, W12523, doi:10.1029/2010WR009111.
- Rollins, R. L., M. G. Spangler, and D. Kirkham (1954), Movement of soil moisture under a thermal gradient, *Highway Res. Board Proc.*, 33, 492–508.
- Rose, D. A., F. Konukcu, and J. W. Gowing (2005), Effect of water table depth on evaporation and salt accumulation from saline groundwater, *Aust. J. Soil Res.*, 43, 565–573, doi:10.1071/SR04051.
- Saito, H., J. Simunek, and B. P. Mohanty (2006), Numerical analysis of coupled water, vapor, and heat transport in the vadose zone, *Vadose Zone J.*, 5, 784–800.

- Salvucci, G. D., and D. Entekhabi (1995), Hillslope and climatic controls on hydrologic fluxes, *Water Resour. Res.*, *31*, 1725–1739, doi:10.1029/95WR00057.
- Saravanapavan, T., and G. D. Salvucci (2000), Analysis of rate-limiting processes in soil evaporation with implications for soil resistance models, *Adv. Water Resour.*, *23*, 493–502, doi:10.1016/S0309-1708(99)00045-7.
- Scherer, G. W. (1990), Theory of drying, *J. Am. Ceram. Soc.*, *73*, 3–14.
- Schlünder, E.-U. (1988), On the mechanism of the constant drying rate period and its relevance to diffusion controlled catalytic gas phase reactions, *Chem. Eng. Sci.*, *43*, 2685–2688, doi:10.1016/0009-2509(88)80012-5.
- Shahraeeni, E., and D. Or (2012), Pore scale mechanisms for enhanced vapor transport through partially saturated porous media, *Water Resour. Res.*, *48*, W05511, doi:10.1029/2011WR011036.
- Shahraeeni, E., P. Lehmann, and D. Or (2012), Coupling of evaporative fluxes from drying porous surfaces with air boundary layer: Characteristics of evaporation from discrete pores, *Water Resour. Res.*, *48*, W09525, doi:10.1029/2012WR011857.
- Shaw, T. M. (1987), Drying as an immiscible displacement process with fluid counterflow, *Phys. Rev. Lett.*, *59*, 1671–1674, doi:10.1103/PhysRevLett.59.1671.
- Shokri, N., and D. Or (2010), Comment on “A simple model for describing hydraulic conductivity in unsaturated porous media accounting for film and capillary flow” by A. Peters and W. Durner, *Water Resour. Res.*, *46*, W06801, doi:10.1029/2009WR008917.
- Shokri, N., and D. Or (2011), What determines drying rates at the onset of diffusion controlled stage-2 evaporation from porous media?, *Water Resour. Res.*, *47*, W09513, doi:10.1029/2010WR010284.
- Shokri, N., and G. D. Salvucci (2011), Evaporation from porous media in the presence of a water table, *Vadose Zone J.*, *10*, doi:10.2136/vzj2011.0027.
- Shokri, N., P. Lehmann, and D. Or (2009), Critical evaluation of enhancement factors for vapor transport through unsaturated porous media, *Water Resour. Res.*, *45*, W10433, doi:10.1029/2009WR007769.
- Simunek, J., M. Th. van Genuchten, and M. Sejna (2005), The HYDRUS-1D software package for simulating the movement of water, heat, and multiple solutes in variably saturated media, *version 3.0*, *HYDRUS Software Ser. 1*, 270 pp., Dep. of Environ. Sci., Univ. of Calif. Riverside, Riverside, Calif.
- Smits, K. M., A. Cihan, V. Ngo, T. Sakaki, and T. H. Illangasekare (2012), An evaluation of models of bare soil evaporation formulated with different land surface boundary conditions and assumptions, *Water Resour. Res.*, *48*, W12526, doi:10.1029/2012WR012113.
- Suzuki, M., and S. Maeda (1968), On the mechanism of drying of granular beds, *J. Chem. Eng. Jpn.*, *1*, 26–31, doi:10.1252/jcej.1.26.
- Taylor, S. A., and L. Cavazza (1954), The movement of soil moisture in response to temperature gradients, *Soil Sci. Soc. Am. J.*, *18*, 351–358.
- Van Brakel, J. (1980), Mass transfer in convective drying, *Adv. Drying*, *1*, 212–267.
- van Genuchten, M. T. (1980), A closed-form equation for predicting the hydraulic conductivity of unsaturated soils, *Soil Sci. Soc. Am. J.*, *44*, 892–898.
- Warrick, A. W. (1988), Additional solutions for steady-state evaporation from a shallow water table, *Soil Sci.*, *146*, 63–66, doi:10.1097/00010694-198808000-00001.
- Whitaker, S. (1998), Coupled transport in multiphase systems. A theory of drying, *Adv. Heat Transfer*, *31*, 1–104.